Hybrid ANFIS Systems: Evaluation Of Bearing Capacity Of Driven Piles

Yan Peng[1*] and Haiquan Gao[2]

[1] Anhui Technical College of Industry and Economy, Hefei, Anhui, 230051, China
[2] CSCEC4 CIVIL ENGINEERING CO.LTD, Hefei, Anhui, 230000, China
[*] Corresponding author. E-mail: pengyan11288@sina.com

Received: Sep. 29, 2024; Accepted: Apr. 04, 2025

Several empirical and theoretical methods have been used in civil infrastructure to ascertain the deep foundation's load capacity. The models in this scenario are primarily driven by physical presumptions as well as the construction of estimations utilizing mathematical frameworks. In this article, innovative design patterns were developed, and three hybrid adaptive neuro-fuzzy inference systems (ANFIS) optimized with artificial rabbit optimization (ARO), cuckoo optimization algorithm (COA), and grey wolf optimization (GWO) have been applied to use experimental data to calculate the driven piles' bearing capacity (Q_t). To increase the optimal networks' modeling efficacy, optimization methods were deployed to determine the essential parameters of the simulations. Also, other algorithms were developed for comparison purposes, such as single ANFIS, support vector regression (SVR) M5P, multi-adaptive regression spline (MARS), random forests (RF), and random trees (RT). It was concluded that both ANFIS systems optimized with ARO, GWO, and COA accomplish admirably among the categories of trains and tests, with a minimum R^2 of 0.9285 in the learning dataset and 0.9313 in the examining dataset, respectively, indicating a strong similarity between experimental and estimated Q_t. Comparing the outcomes of the single and hybrid models, the highest performance belonged to ARO-ANFIS, by gaining the largest values of correlation metrics and the lowest values of error-based metrics. After examining the dependability and considering the justifications, the ANFIS paired with ARO outperformed the COA-ANFIS and GWOANFIS in the Qt of driven piles forecasting model, this is the suggested system.

Keywords: Driven piles; Bearing capacity; Evaluation; Deep foundation; ANFIS; artificial rabbit optimization

http://dx.doi.org/10.6180/jase.202602_29(2).0023

1. Introduction

Engineering, particularly geotechnical engineering, uses empirical and non-empirical methods to calculate deep foundation-bearing capacity [1–3]. The models in this scenario are mainly driven by physical assumptions and the process of constructing estimates using algebraic concepts [4–6]. Calculating non-shallow foundations' bearing capacities is one of the most challenging problems in geotechnics to tackle [7–9]. It is typical to discover a variety of methods to complete this task in the research; however, the precision of such answers is generally imprecise due to factors such as the fact that some equations were calculated empirically or unofficially. Foundations are the linking sections accountable for maintaining any ground-level buildings [10]. A foundation, is a network made up of the soil's many layers that surround and support the foundation as well as its structural components. The portion of the building that is in charge of receiving and distributing loads from the structure to the rock or bottom soil is known as the foundation on which the construction is built [10–12]. According to Bowles, the soil should be susceptible to sustaining like loads with no failing or settling to an unacceptable as well as unfavorable degree, taking its intended use into account [10]. The building of foundations often necessitates knowledge of both the behavior and stress-related compressibility of soils and the geological formations of the soils, which

will underpin the foundation in order to meet these requirements [13]. The two main categories of structures that they support are shallow foundations and deep foundations in most circumstances. The classification rules adopted by different authors may vary, even if they are based on the same assumptions. Shallow bases contain a depth more minor than the base dimension, but deep foundations possess a base length of more than four times the base dimension [10]. A deep foundation is also one whose base fracture process does not extend to the ground level. In terms of the second-largest team, Vesic [14] distinguishes between two different kinds of deep foundations: the first are foundations implemented through excavation or drilling that do not provoke meaningful alterations in the adjoined soil, as well as the second are foundations pressured into the surface through activities like driving that induce substantial improvements in bearing soil. The maximum carrying capacity of the deep must be taken into account [14]. The ultimate capacities of an isolated pile might well be determined using one of three methods: static formulas, dynamic equations, or load trials. Despite much mathematical and practical research into pile behavior and bearing capacity, their mechanisms remain a mystery [13, 15]. Multiple the pile point capacity by soil-pile skin friction to get the final bearing capacity [7, 13]. According to Bowles [10], obtaining a prognostication of capacity close to real load exam values through its use is not a common occurrence. A lack of correspondence can occur due to problems evaluating in-situ soil properties and their variations in the pile's proximity just after installation. Because of the inherent heterogeneity of soil and the complex pile-soil interactions, accurate planning is difficult [10]. Fuzzy systems, ANN s (Artificial neural networks) as well as other machine learning methods have been shown to be helpful in solving a variety of engineering problems [9, 15–22]. A comprehensive study of the applicability of ANN s in geotechnical engineering was published [23]. ANNs has been implemented to simulate pile settlement [24–26], UBC [27], piles' lateral deflection [28], the capacity of pile dynamic [29], as well as the drivability of piles [30]. Goh [31] employed ANN methods to calculate the UBC of piles. The testing and teaching data's regression coefficients of 0.96 and 0.97, in that order, show that their suggested model can compute UBC. To anticipate the pile capacity using cone penetration test (CPT) and CPTu data, Ardalan et al. [32] employed polynomial ANN s and genetic algorithms. It was shown that the highest efficient solution could properly forecast the pile capacity. Alkroosh et al. used the least-square support vector machine technique to calculate the drilled piles' UBC [33]. Traditional CPT and gene expression programming (GEP) methodologies were contrasted with the model's outcomes. UBC estimations were better predicted using this method than traditional methods, according to the model's performance metrics. To estimate the UBC of piles, Milad et al. [34] employed soft computing methods like genetic programming, linear regression, as well as ANN s, and then compared the results. The analysis indicates that the ANN performed the best when it came to predicting UBC values. Using 36 pile drive analyzer tests, a computer system was developed by Milad et al. [34] to forecast tip resistance and concrete piles. The top ANN model has correlation coefficients of 0.941, 0.936 , and 0.951 for learning, verifying, and assessing data. This shows that their proposed approach may properly identify resistances at the shaft and tip.

The friction barrier of piles in clay soil was measured by Suman et al. [35]. MARS (Multivariate adaptive regression splines) and FN (functional networks) were employed as computer simulations, and their performance indicators were compared to those of the existing systems. The networks were validated on experimental observations, as well as the results showed that MARS and FN were more resistant to predicting than earlier models. Maizir [36] forecasted the piles' bearing capacity utilizing several MLP simulations. The pile-driving inquiry data were utilized to train the model. The most powerful algorithm predicted pile shaft bearing capacity based on their data. Artificial Intelligence (AI) design charts were used to determine a pile's capacity friction in clay soil [37]. The investigators utilized a range of nonlinear modeling approaches in their investigation. The inputs to the models were the soil's effective stress and undrained shear strength, as well as the pile shapes, and the purpose was to ascertain the soil's capacity for friction. The accuracy of the ANFIS model ($\mathrm{R} = 0.97$) is superior to that of the SVM($\mathrm{R} = 0.89$) as well as GP($\mathrm{R} = 0.95$) models. To determine the friction ability of piles on sandy soil, Moayedi and Hayati [37] used a friction capacity ratio calculator. Particle swarm optimization and two genetic algorithms improved the performance of the ANFIS model. According to the decision, the friction capacity ratio would be the model's goal. In their analysis, they discovered that the ANFIS - GA model possessed improved performance metrics regarding R^2 as well as $RMSE$. The research used Terzaghi's equations to predict soil carrying capacity using index characteristics, shear strength, and relative depths. MLR (Multiple linear regression) was utilized to create the model utilizing 30 data sets, and natural bearing capacity was accurately predicted. Strip, square, and circular footings had R^2 values of 96.98%, 96.93%, and 96.90%, indicating strong model dependability [38]. The idea was to optimize the configuration of the ANN hy-

bridized optimization algorithms for soil-bearing capacity analysis. Applied stress was discovered as the most important input factor through an unbiased predictor. As the results indicated, due to the lowest value of $RMSE$ and MAE, and the highest value of correlation, the electrostatic discharge algorithm (ESDA) $-$ ANN model approximated the training and testing datasets slightly better than the others [39]. A publication provided a hybrid model that predicted concrete pile bearing capacity using the whale optimization algorithm (WOA) and extreme gradient boosting machine (XGB). The WOA, which finds the best XGB settings, improves model accuracy and resilience. Our hybrid model continuously outperformed deep neural network (DNN) regression and the XGB model by default. In 20 trials, the suggested model reduced RMSE by 12,11.7, 9, and 12% as opposed to the DNN's 2, 3, 4, and 5 hidden layer [40].

It has been discovered that the artificial rabbit optimization (ARO), cuckoo optimization algorithm (COA) and grey wolf optimization (GWO) have a positive impact on the coupling between ANFIS systems [40–43]; So that innovative design patterns may be developed, two hybrid ANFIS models optimized with ARO, COA and GWO have been applied in the current essay to calculate driven piles' bearing capacities using experimental data. This has allowed for the development of distinctive models of design. To increase the optimal networks' modeling efficacy, optimization methods were deployed to determine the essential parameters of the simulations, which were then applied. To evaluate the optimal model's performance, new experimental tests and classic equations were conducted.

Optimizing the structures of ANFIS models compared to other AI models can offer several advantages:

- Optimizing the structure of an ANFIS model can lead to improved accuracy in predictions or classifications. By fine-tuning the architecture, the underlying patterns in the data can be more accurately captured by the model, resulting in enhanced performance.

- Optimization can help in simplifying the structure of the ANFIS model by eliminating unnecessary nodes or connections. A more streamlined architecture not only improves computational efficiency but also makes the model easier to interpret and understand.

- An optimized structure can lead to faster convergence during the training process. When working with big datasets or intricate models, this is especially crucial, as it reduces the computational time required to train the ANFIS.

- When a model is very complicated and fits the training data too closely, it is said to be overfitting and performs badly when applied to new data. Optimizing the structure helps prevent overfitting by finding the right balance between model complexity and generalization.

- Optimization can lead to more efficient use of computational resources, making the ANFIS model suitable for deployment in real-time applications or on resource-constrained devices.

- The selection of optimization algorithms was based on their strengths in handling complex, nonlinear optimization problems. ARO is adept at balancing exploration (searching for new solutions) and exploitation (refining existing solutions). This balance makes it particularly effective for complex scenarios where avoiding local optima is critical. COA is known for its ability to escape local optima through a combination of Lévy flight and targeted solution replacement. GWO offers robust convergence capabilities by incorporating leader-driven solution refinement and diverse exploration phases, where its simplicity and efficiency make it widely used in engineering applications. These algorithms were chosen because of their complementary approaches to optimization, ensuring diverse exploration of the solution space and effective convergence to global optima.

2. Methodology

2.1. Data collection and properties

As previously mentioned, in order to assess the validity of the final capacity estimations obtained, the research compares load capacity guesses estimated using algorithms using field load testing-derived load capacities. The suggested methodology was assessed utilizing indicators dependent on the model's results and field values and compared to real-world load test results. Load capacity, hammer weight, hammer drop height, pile length, and pile diameter were all included in the project's set of 232 load tests done in different countries in the world [44–46]. The data accumulation includes load experiments reported in the literature and load tests in the authors' professional work according to related standards [47, 48]. To measure a network's load capacity (Q_t), variables such as hammer drop height (H), hammer weight (W), pile diameter (D), pile length (L), permanent penetration of a pile formed by the final hammer blow (S), and modulus of elasticity (E_p) served as the input data. 75% of the data was utilized

for each neural network training, while the remaining 25% was utilized to assess and validate the topology [49–51]. The gathered data, and even the architecture of the systems and their attributes, will be displayed in charts and tables. Table 1 and Fig. 1 depict the features of parameters used in the creation of algorithms as well as their distribution.

A statistical tool utilized to measure the direction and strength of a linear relationship between two continuous variables is the Pearson correlation coefficient. It assesses how much one variable tends to change when the other variable changes. To calculate this coefficient, the variables were standardized by subtracting their means and dividing by their standard deviations. Then, the average of the product of these standardized values was computed across all observations. The coefficient ranges from -1 to 1 , where 1 signifies a perfect positive linear relationship (both variables increase together), -1 signifies a perfect negative linear relationship (one variable decreases as the other increases), and 0 indicates no linear relationship. It's critical to understand that linear relationships are the only ones that the Pearson correlation coefficient measures and may not capture nonlinear associations or relationships influenced by outliers. According to the result for Q_t, Fig. 2 illustrates that this coefficient among any two components is small (i.e., < 0.485), which implies that these features rarely cause multicollinearity difficulties [52]. Between the variables, there are the largest positive correlations between Q_t and D at 0.826 , followed by W and D at 0.803 , which shows both variables increase together.

2.2. Models

2.3. COA

The values of decision variables must first be displayed in an array in order to resolve optimization problems. We call this array "habitat" in the cuckoo optimization method. As a result, every natural environment will act as a nominee answer to an optimization issue. Within an evolutionary procedure, nominee answers converge to a globally optimum answer. The natural environment will be an array of $1 \times N_{\text{var}}$ dimensions in an N_{var} decision variablebased optimization issue means environment $= [x_1, x_2, x_3, \ldots, x_{N_{var}}]$. The cuckoo's spatial coordinates within the decision area are displayed in this array. The benefit of the natural environment is calculated by assessing these values for every natural environment utilizing the benefit function (f_p) (profit $= f_p($ habitat $))$. Decision variable values are decimal. The cost function (f_c) is able to simply be decreased by maximizing the benefit function in Eq. (1) since this method is primarily designed for benefit maximization issues [53].

$$\text{rofit } = -\text{cost}(\text{ habitat }) = -f_c\left(x_1, x_2, x_3, \ldots, x_{N_{\text{var}}}\right) \quad (1)$$

The following is the Cuckoo optimization method evolutionary procedure: A $N_{\text{pop}} \times N_{\text{var}}$ matrix of nominee natural environments is initially built after specifying the starting crowd of cuckoos (N_{pop}). So an accidental number of cuckoo eggs are collected from every built natural environment. In nature, every cuckoo has a number between 5 and 20 on average. The maximum and minimum eggs' number allowed in every natural environment are represented by these numbers. In reality, of course, cuckoos discard their eggs as far away from their natural environments as possible. This most significant interval is referred to as the egglaying radius in the cuckoo method. The egg-laying radius for each cuckoo is specified using Eq. (Eq. (2)), and the total quantity of eggs, as well as the lower (Var $_{\text{low}}$) and higher limits (Var_{high}) of the decision variable values. The integer parameter denoted as α, is utilized to control the egg-laying radius's maximum value.

$$ELR = \alpha \times \frac{\text{No.of.Current,Cuckoo's.Eggs}}{\text{Total.Nmuber.of.Eggs}} \times \left(\text{var}_{\text{high}} - \text{var}_{\text{low}}\right) \quad (2)$$

In the following phase, every cuckoo randomly dumps one egg in the host bird's lair within its egg-laying radius. When the egg-laying procedure is completed, the host bird detects and eliminates the eggs that are not identical to those of the host bird. Hence, some cuckoo eggs (which may account for a percentage of the eggs) vanish after every egg-laying procedure. These eggs can't converge on an optimal answer since they are in a low food resource habitat. Other eggs develop, hatch, as well as are fed by the host bird while they remain in its lair.

Cuckoo chicks stay in their environment after they have grown up for a while; however, by the time they're ready to lay eggs, they have moved to places with more significant food resources on the one side, as well as their egg pattern and color closely resemble those of the host bird in that area on the other side. Cuckoo migration will settle in societies with the most significant benefit margins (the food resources and the greatest living situations). Given that adult cuckoos are sparingly distributed throughout their habitats, determining which society every cuckoo belongs to is challenging. The cuckoos are grouped using the K-means clustering technique to dissolve this issue. After determining every cuckoo cluster, the mean benefit for every cluster is appraised. The finest environment is available in the cuckoo cluster with the greatest mean production.

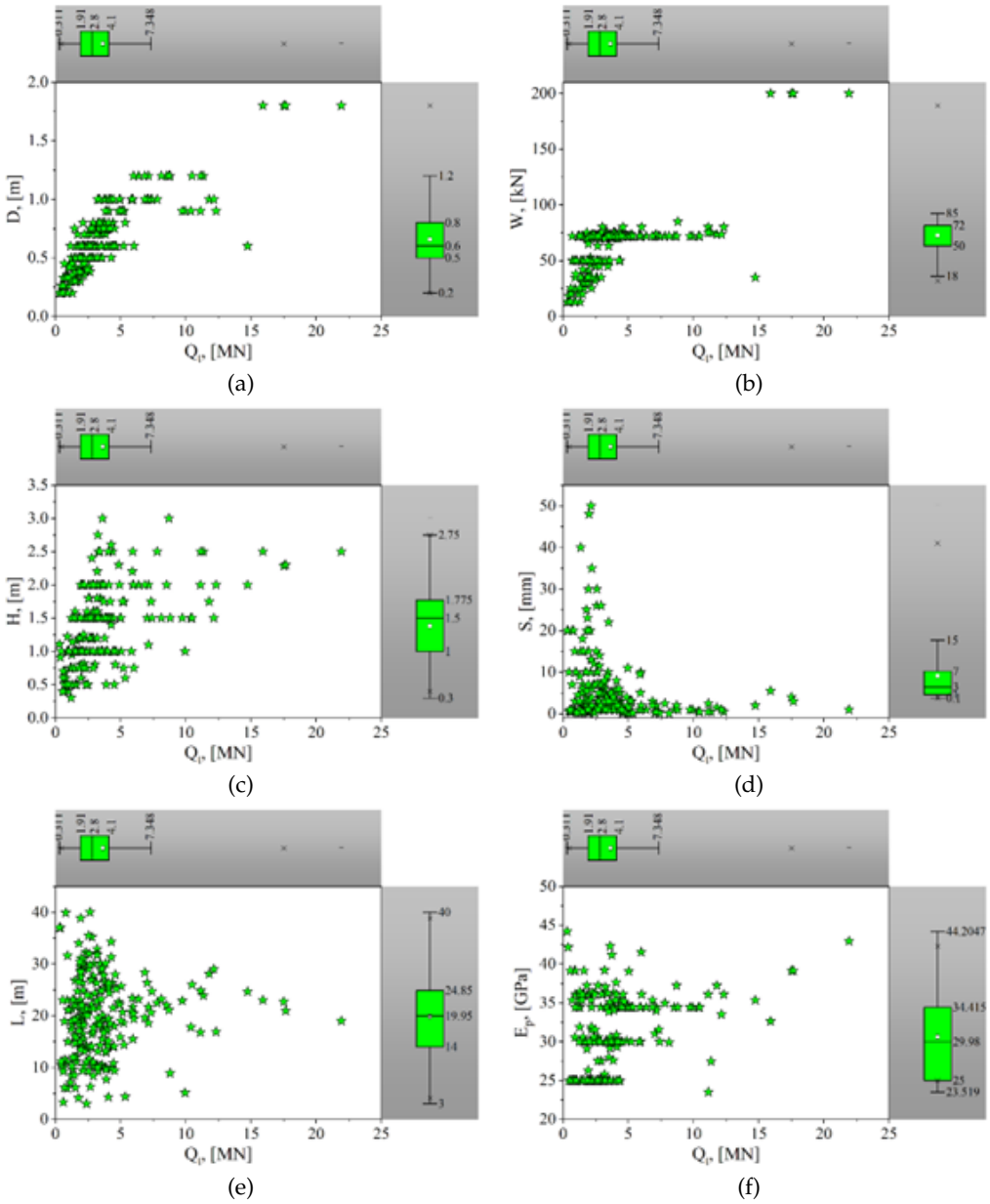

Fig. 1. The input's distribution versus Q_t

Table 1. The characteristics of variables used to build models

		Inputs						Output
Data	Index	D	W	H	s	L	E_p	Q_t
		m	kN	m	mm	m	GPa	MN
	Max.	1.80	200.0	3.0	50.0	40.0	42.9450	21.9230
	Min.	0.20	13.0	0.30	0.10	3.30	25.0	0.3870
	Median	0.60	72.0	1.450	3.0	19.30	29.980	2.850
Train set	Avg.	0.6530	60.3520	1.3800	5.4590	19.6440	30.4850	3.6830
	Skew.	1.1880	2.1880	0.4130	3.1470	0.1790	0.3380	2.7720
	St.d.	0.2850	26.2210	0.5550	7.8910	7.7480	4.9980	3.2180
	Kur.	2.8290	11.9910	-0.3570	12.1280	-0.5220	-1.0780	9.6710
	Max.	1.80	200.0	3.0	35.0	39.90	44.20470	15.9180
	Min.	0.20	13.0	0.3970	0.10	3.0	23.5190	0.3110
	Median	0.60	72.0	1.50	2.750	21.1250	30.2750	2.6750
Test set	Avg.	0.6710	63.0430	1.3800	6.6140	20.3940	30.8960	3.5790
	Skew.	1.2040	2.1420	0.4630	1.6770	-0.0190	0.2630	2.0820
	St.d.	0.3040	25.5870	0.6150	7.8830	7.8070	5.1080	2.8830
	Kur.	2.0330	13.3680	-0.3870	2.4570	0.0640	-0.8240	5.4160

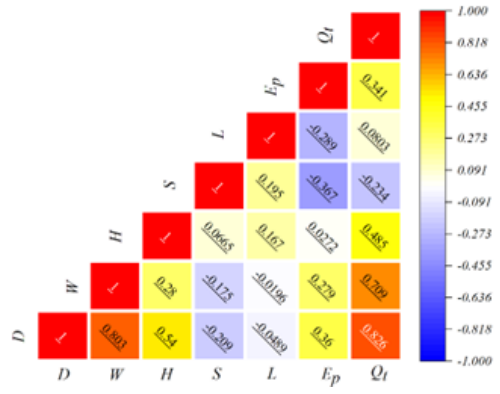

Fig. 2. The input attribute-corresponding correlation matrix

Other cuckoo groups have chosen this area as a target habitat and immigration location. Cuckoos do not go through the target natural environment; instead, they move via selected portions of the destination with a certain deflection. It should be noted that owing to the inadequate availability of food, cuckoos get hunted, and the occasional absence of a proper lair for the growth of chickens, it is necessary to implement a cuckoo population control parameter. Only the $N_{\max}$ Cuckoos, which provide the maximum benefit, remain alive in the COA for this reason. Entire cuckoo populations converge to the finest natural environment in the ecosystem after multiple iterations in the COA. The host birds' eggs, which have the richest food supplies in this ecology, will most closely resemble those of the cuckoo.

2.4. Gray wolf optimization (GWO)

GWO has effective specifications containing too few adjusting parameters, easy usability, simplicity, flexibility, scalability, and the right balance between the exploitation and exploration during the time of exploring conducting to desirable isotropy [54]. GWO is according to the grey wolves' social ranking. There exist four kinds of ranking named α, β, δ and ω, for reducing superiority. The finest answer is gained by the alpha wolf. The preying via exploring, surrounding, and striking the hunt is modeled to discover the optimal answer by balancing exploitation and exploration.

$$\vec{D}_\omega = \left|\vec{C}_\omega * \vec{X}_p(t)\vec{X}_\omega(t)\right| \tag{3}$$

$$\vec{X}_{\omega,lgw}(t) = \vec{X}_p(t) - \vec{A}_\omega * \vec{D}_\omega \tag{4}$$

In the equations above, $\overrightarrow{X_p}$ stands for the target hunt's situation vector, t shows the present iteration, $X_{\omega,lgw}$ shows a present plausible situation vector of ω wolf following every conducting grey wolf, $\vec{X}_\omega(t)$ shows the present situation of the ω wolf, D_ω shows the interval of the ω wolf from a hunt or even conducting wolves determining the hunt's perspectives. $\vec{X}_{\omega,lgw}$ is replaced by $\vec{X}_{\omega,\alpha}$, $\vec{X}_{\omega,\beta}$, and $\vec{X}_{\omega,\delta}$ when hunt position X_p is replaced by X_β, X_δ, and X_α, respectively. The coefficient vector overrightarrow A_ω and overrightarrow C_ω in order to every one of the ω wolves are computed as below.

$$\vec{A}_\omega = 2\vec{a} * \overrightarrow{r_1} - \vec{a} \tag{5}$$

$$\vec{C}_\omega = 2 * \overrightarrow{r_2} \tag{6}$$

$$\vec{X}_\omega(t+1) = \left(\vec{X}_{\omega,\alpha}(t) + \vec{X}_{\omega,\beta}(t) + \vec{X}_{\omega,\delta}(t)\right) \tag{7}$$

In Eqs. (Eq. (5)) and (Eq. (6)), $\vec{a}$ is linearly reduced from 2 to 0 while the iterations' term $(2.0(1t/T)$), where T shows the iterations' maximum number, t shows the present iteration, and $\vec{r}_1, \vec{r}_2$ denotes a vector organized by accidental values among 0 and 1 discussing the issue dimension. The hunt's position as the optimum value of the answer is firstly not recognized. However, the initial three answers generating the finest suitable values are intended as α, β and δ wolves assumed to have the futuristic knowledge about hunt positions according to the ranking. The actual update of entirely different grey wolves (ω) determined by $\vec{X}_\omega(t+1)$ is carried out by obtaining the arithmetic average of the perspective answers readjust utilizing Eq. (Eq. (4)) with perspective to these three wolves. This is presented in Eq. (7). The hunting treatment of the grey wolves is simulated by contemplating that α, β and δ wolves are near the prey.

2.5. Artificial rabbit optimization (ARO)

The protective strategies used by rabbits in the wild are mathematically described and integrated into an effective optimizing mechanism in the proposed ARO. This method handles two simulation techniques: random concealment and detour foraging. As part of the detour foraging strategy, the rabbit is compelled to consume the grasses near other people's nests, which may prevent attackers from discovering its nest. Furthermore, a rabbit may choose randomly to hide in any of its own shelters by using the randomized concealment strategy, which may reduce the possibility that its enemies may seize it. Furthermore, when their energy levels dropped, the rabbits would turn from their detour foraging technique to their random concealment technique [55].

Each repetition updates the position of every population bunny according to the rules of the proposed algorithm, which is then assessed by the fitness function. As the technique proceeds, the solutions become more refined. The formula (8) assigns any beginning population site to a unique place inside the searching region:

$$Y_i = lb + [ub - lb] \times \text{rand}(1, \text{dim}) i = 1, 2, \ldots, n \tag{8}$$

The variable Y_i represents the location of the animal lb and ub represent the maximum and minimum values of the variables being evaluated, and n and dim respectively represent the population size and the number of control parameters in the issue.

Each seeking individual chooses to alter its relative position to a different searching individual chosen at random from the swarming and combined perturbation, based on the ARO's detour foraging behavior. The intended mathematical explanation of the bunnies' detour foraging is as follows:

$$\begin{aligned} &R_i(it+1) = Y_j(it) + Z \times \left(Y_i(it) - Y_j(it)\right) + \text{rand} \\ &(0.5 \times (0.05 + v_1)) \times \\ &\text{SND}, \quad i, j = 1, \ldots, j \neq i \end{aligned} \tag{9}$$

$$Z = c \times L \tag{10}$$

$$\begin{aligned} &c(k) = \begin{cases} 1 \text{ if } k = g(1) \\ 0 \text{ else} \end{cases} \\ &, k = 1, \ldots, \text{ dim and } l = 1, \ldots, [v_2, \text{ dim }] \end{aligned} \tag{11}$$

$$g = \text{ randperm } (d), n_1 \sim N(0,1) \tag{12}$$

$$L = \sin(2\pi v_3) \times \left(e - e^{((it-1)/T_{\max})^2}\right) \tag{13}$$

When the time is referring to the present moment, the new and ancient bunny locations are R_i and Y_i, respectively; The standard normal distribution controls SND, and the distance traveled, denoted as L, represents the velocity. Here are three randomized numbers within the range of $[0,1]$: v_1, v_2, and v_3.$T_{\max}$ is the maximum number of iterations. round and randperm are functions that round the result to the nearest integer and randomly permute the numbers from 1 to dim.

In order to have shelter while escaping from adversaries, rabbits often look for tunnels next to their nest. An additional formula is given in this regard.

$$\begin{aligned} b_{i,j}(it) =& Y_i(it) + H.G.Y_i(it), \\ & i = 1, \ldots, n \text{ and } j = 1, \ldots, \text{dim} \end{aligned} \tag{14}$$

$$H = \frac{T_{\max} + 1 - it}{T_{\max}} \times v_4 \tag{15}$$

$$G(k) = \begin{cases} 1 \text{ if } k = j \\ 0 \text{ else} \end{cases} \quad k = 1, \ldots, \text{dim} \tag{16}$$

v_4 is a randomly assigned value between 0 and 1 , and $b_{i,j}$ is the jth rabbit burrow (i). The hiding parameter, H, increases from 1 to $1/T_{\max}$ with a random perturbation over repetitions. This trait determines where a rabbit will

dig its initial burrow, which is usually in its wider neighborhood. The more iterations there are, the smaller this neighborhood becomes.

To live, rabbits need to find a safe location to hide. As a result, they're disinclined to choose a hole among many they must hide in at random in order to escape being found. The random concealing technique can be expressed mathematically in the following way:

$$R_i(it+1) = Y_i(it) + Z \times \left(v_5 \times b_{i,j}(t) - Y_i(it)\right) \quad i = 1, \ldots, n \tag{17}$$

The location of the ith bunny is modified in the following manner once either randomized hiding or detour foraging is successful:

$$Y_i(it+1) = \begin{cases} Y_i(it) & f\left(Y_i(it)\right) \leq f\left(R_i(it+1)\right) \\ R_i(it+1) & f\left(Y_i(it)\right) > f\left(R_i(it+1)\right) \end{cases} \tag{18}$$

The process of transitioning from the first stage of detour foraging to the subsequent stage of randomized concealment involves including an energy factor. The following explanations pertain to the energy component inside this formula:

$$A(it) = 4\left(1 - \frac{it}{T_{\max}}\right) \ln \frac{1}{r} \tag{19}$$

2.6. ANFIS (Adaptive neuro-fuzzy inference system)

The ANFIS is recognized as a hybrid machine learning method utilized in order to accurately plan the solidarity that exists among the affiliate and forecaster variables [56]. The ANFIS contains the ANN and fuzzy logic's profits to get better the forecast and learning abilities of the network.

The ANFIS's fundamental architecture contained with Takagi, Sugeno, and Kang (TSK) rule basis learning methods for two inputs (X, Y) and a single result (y) is presented in Fig. 3 Presume that the ANFIS rule basis structure considering two _then TSK's rules [57].

Rules 1: If $(X \text{ is } A_1)$ and (Y is B_1) then $y_1 = \alpha_1 X + \beta_1 Y + \gamma_1$

Rule 2: If $(X \text{ is } A_2)$ and (Y is B_2) then $y_2 = \alpha_2 X + \beta_2 Y + \gamma_2$

In the equations above, γ, β and α are discussed as linear resulting parameters and A_1, B_1, A_2 and B_2 are the preconditioned linguistic terms of fuzzy logic. The ANFIS network's functionality, including five substrate architectures, is defined as below:

- Substrate 1 (fuzzy substrate): in the fuzzy substrate, the membership functions and their rates (linguistic terms) in order to the presented input crisp input (X, Y) have been allocated. This fuzzy substrate's result is able to be presented as:

$$O_{ij}^1 = \varphi_{ij}(X, Y), i = 1, \ldots, m \text{ and } j = 1, \ldots, n \tag{20}$$

In this equation, φ_{ij} stands for the proper membership function for the input variables Y and X. The variables defined in substrate one are mentioned as hypothesis parameters, which could differ with several membership functions.

- Substrate 2 (Product substrate): in the product substrate, the input signals from substrate one have been multiplied with the prod t-norm factor in order to synthesize enough data for a subsequent substrate. The result of the product substrate
in a mathematical way is able to be observed below:

$$O_i^2 = \varphi_i(X).\varphi_i(Y) \tag{21}$$

- Substrate 3 (Normalized substrate): every node dataset gained from the product substrate is normalized by allocating weight function to get better every fuzzy rule's firing power, the mathematical way for summation of firing power of i^{th} the rule is presented below:

$$O_i^3 = \bar{\psi} = \frac{\psi_i}{\psi_1 + \psi_2} \tag{22}$$

- Substrate 4 (Adaptive or de-fuzzify substrate): the defuzzified result of the presented crisp result is able to be observed by the equation below:

$$O_i^4 = \overline{\psi_i} f_i = \overline{\psi_i}\left(\alpha_i X + \beta_i Y + \gamma_i\right) \tag{23}$$

In the equation above, γ, β and α are the ANFIS network's resulting parameters.

- Substrate 5 (result substrate): in substrate 5, the ANFIS's cumulative result is synthesized utilizing the de-fuzzified substrate's result and presented as the fixed function below.

$$O_i^5 = \sum_{i=1}^{n} \overline{\psi_i} f_i \tag{24}$$

The resulting parameters' linear mixture is gained as the last result of the learned ANFIS network.

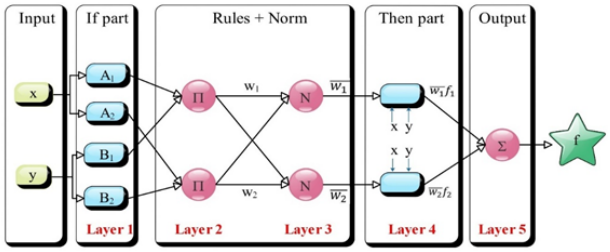

Fig. 3. Architecture of ANFIS

2.7. Coupled ANFISs

The ANFIS is a powerful hybrid model that combines the adaptability of neural networks with the interpretability of fuzzy logic. Developing an ANFIS model involved several key steps, including:

- The dataset containing input-output pairs was gathered. The data was preprocessed by handling missing values, normalizing or standardizing features, and splitting them into training and testing sets.
- The fuzzy inference system was defined, including the number of fuzzy sets and their membership functions for each input variable. This step involves linguistic modeling, where domain experts may provide insights into the membership functions and fuzzy rules.
- The membership functions' parameters were initialized.
- The ANFIS model was trained using a hybrid learning algorithm, where RMSE index was considered as an objective function.
- The initially developed model was reconstructed by linking with optimization algorithms in order to raise the prediction accuracy and pace. In the present study, the ARO, COA, and GWO algorithms were coupled with ANFIS for these purposes (abbreviated as ARO - ANFIS, COA - ANFIS and GWO - ANFIS). The trained hybrid ANFIS models were evaluated using the testing dataset. By tuning hyperparameters with optimization algorithms, it can be enhanced the performance and generalization capability of ANFIS models, ultimately, improving their accuracy and robustness for real-world applications. The initialized and tunned values of parameters are provided in section 2.7.

The computational efficiency of machine learning models is an important criterion for evaluating their practicality, especially for large-scale or real-time applications. In this study, the computation time required for training and testing each model was recorded. The results are summarized in Table 3.

The analysis reveals that between single models, the SVR model demonstrated the shortest total computation time of 30.1 seconds, making it the most computationally efficient among the tested models. In contrast, the ANFIS model required the longest time (94.0 seconds) due to the higher complexity of its structure and optimization process. Regarding the hybrid algorithms, ARO - ANFIS resulted the moderate second, but larger than single ones. The observed variation in computation times is attributed to differences in model architecture, optimization algorithms, and dataset size. While computational efficiency is important, it should be balanced with accuracy, as some models with higher computation times may yield more accurate predictions.

2.8. Evaluators

The following quantitative metrics can be used to assess the modeling's dependability (a) Squared Coefficient of correlation (R^2) (Eq. (27)), (b) RMSE error (Root mean squared) (Eq. (28)), (c) Mean absolute error (MAE) (Eq. (29)), (d) Relative Absolute Error (RAE) (Eq. (30)),root relative squared error Error (RRSE) (Eq. (31)), and scatter index (SI) (Eq. (32)).

$$R^2 = \left(\frac{\sum_{d=1}^{D} (m_d - \bar{m})(z_d - \bar{z})}{\sqrt{\left[\sum_{d=1}^{D} (m_P - m)^2\right]\left[\sum_{d=1}^{D} (z_d - \bar{z})^2\right]}} \right)^2 \quad (25)$$

$$RMSE = \sqrt{\frac{1}{D}\sum_{d=1}^{D} (z_d - m_d)^2} \quad (26)$$

$$MAE = \frac{1}{D}\sum_{d=1}^{D} |z_d - m_d| \quad (27)$$

$$RAE = \frac{\sum_{d=1}^{D} |m_d - z_d|}{\sum_{d=1}^{D} |m_d - \bar{m}|} \quad (28)$$

$$RRSE = \sqrt{\frac{\sum_{d=1}^{D} (m_d - z_d)^2}{\sum_{d=1}^{D} (m_d - \bar{m})^2}} \quad (29)$$

$$SI = \frac{\sqrt{\left(\frac{1}{P}\right)\sum_{p=1}^{P} \left((y_p - \bar{y}) - (t_P - \bar{t})\right)^2}}{\left(\frac{1}{P}\right)\sum_{p=1}^{P} t_p} \quad (30)$$

D is the number of data collected; m_P and $\bar{m}$ are the actual values and their average; z_P and $\bar{z}$ are the simulated values and their average; and so on.

Table 2. The initialization procedure and tunned values

Methods	Principal or tunned terms	Initial or tunned values
COA	Maximum iteration number	100
	Count of runs	10
	Quantity of populations	30
	Levy Flight Exponent	[1, 3]
GWO	Maximum iteration count	100
	Count of runs	10
	Quantity of populations	40
	a	[2, 0]
ARO	Maximum iterations count	100
	Count of runs	10
	Quantity of populations	45
COA - ANFIS	The total count of fuzzy rules	15
	The total count of MFs	24
	Epoch number	40
	Type of MF	trimf
	Shape of fuzzy developed structure	Sugeno
GWO-ANFIS	The total count of fuzzy rules	18
	The total count of MFs	23
	Epoch number	40
	Type of MF	trimf
	Shape of fuzzy developed structure	Sugeno
ARO-ANFIS	The total count of fuzzy rules	32
	The total count of MFs	28
	Epoch number	40
	Type of MF	trimf
	Shape of fuzzy developed structure	Sugeno

Table 3. Computation time for each model

Model	Total Time (s)	Model	Total Time (s)	Model	Total Time (s)
ANFIS	94.0	ARO - ANFIS	139.2	RF	38.4
COA - ANFIS	178.3	M5P	58.0	RT	45.6
GWO - ANFIS	112.4	MARS	50.0	SVR	30.1

3. Results and justifications

In the present essay, to develop innovative design patterns, three hybrids ANFIS models optimized with ARO, COA, and GWO have been applied in the current article that uses experimental data to calculate driven pile bearing capacity. This has allowed for the development of unique design models. To increase the optimal networks' modeling efficacy, optimization methods were deployed to determine the essential parameters of the simulations, which were then applied.

The implications of the blended ANFIS systems, abbreviated as ARO - ANFIS, COA - ANFIS, and GWO - ANFIS, to determine the driven piles Q_t 's load capability was collated and argued in the following part. After much deliberation, it was decided to divide the data into two subgroups at random: an analyzing portion and a training part, with 25 and 75% of the sample allocated between them. Fig. 4 indicates the interaction between the produced and real Q_t. Fig. 5 presents the violin plots of the three developed models. In order to justify the robustness and reliability of creating networks, several reasoning criteria have been examined and investigated in data mining research. A number of measures, including R^2, RMSE, MAE, RAE, and RRSE, were compared and computed in order to reach this superiority (Table 4). An additional scoring method was devised to find the best framework based on the summing of received ranking scores (TRS), where the value of R^2 is higher, and as MAE, RMSE, RAE, and RRSE are lower, the allocated score will be significant. In order for extra validation, six single algorithms were also developed, such as single $ANFIS$, $M5P$, MARS, RF, RT, and SVR.

In addition to quantitative productivity indicators like R^2, $RMSE$, MAE, RAE, and RRSE, it is evident that both ANFIS systems optimized with ARO, GWO and COA accomplish admirably in categories of the test and train, with a minimum R^2 of 0.9285 in the learning dataset and 0.9313 in the examining dataset, respectively, indicating a strong similarity between experimental and estimated Q_t. Com-

paring the results of the single and hybrid models, it is obvious that the highest performance belonged to ARO - ANFIS, by gaining the largest values of correlation metrics and the lowest values of error-based metrics. The values of R^2 for outperformed model equal to 0.9882 and 0.98 related to $ARO - ANFIS$ for the training and testing stages, respectively. Considering other error-based metrics, the same behavior is validated with superiority of ARO - ANFIS, by receiving smaller values of RMSE, MAE, RAE, RRSE, and SI respect to other models. Regarding the second-best model, it is clear that the GWO - ANFIS system's results are near to the best model with slight differences, followed by COA - ANFIS. Although the COA - ANFIS's performance was weaker than the other two hybrid ANFIS models, its accuracy was higher than single ANFIS and the single analysis.

The error percentage distribution plots for developed models in the testing and training phases are provided in Fig. 6 These plots provide a visual representation of the accuracy of prediction methods by showing the distribution of prediction errors. By observing the spread and shape of the distribution, one can gain insights into the magnitudes of errors produced by the prediction method. These plots facilitate comparison between different prediction methods. Also, error percentage distribution plots can be used as a quality assurance tool during model development and validation. Deviations from expected error distributions can indicate potential issues with the model or the data. It is worth mentioning that the narrower the distribution with a higher peak point, the higher the accuracy. It is obvious from this figure that the ARO ANFIS system concluded the best performance by narrower distribution and restricted upper and lower bounds. After this, the performance of GWO - ANFIS is roughly similar to ARO - ANFIS but slightly weaker. Finally, the workability of the COA - ANFIS depicted the wider normal distribution and smaller peak point around zero percentage.

A Taylor diagram is a graphical tool used for assessing the performance of prediction methods, particularly in comparison to a reference dataset. The purpose of a Taylor diagram is to visually represent how well a set of predictions matches the observed data across multiple statistical metrics simultaneously. Taylor diagrams allow for the simultaneous comparison of multiple statistical metrics, like root mean square error (RMSE), correlation coefficient, and standard deviation. This provides a comprehensive assessment of prediction accuracy beyond a single metric, giving a more nuanced understanding of model performance. Moreover, Taylor diagrams facilitate the comparison of multiple prediction methods on the same plot, making it easy to see which method performs better regarding accuracy and variability across different metrics. When developing prediction models, Taylor diagrams can be used to assess the impact of model improvements or parameter tuning by comparing diagrams before and after the changes. The developed models' comparison is provided in the Taylor diagram for the training and testing stages (Fig. 7). The closer the point to the reference point, the higher the accuracy. It is understandable from these figures that the ARO - ANFIS could obtain a closer point to the reference point in both train and test stages, than GWO - ANFIS, followed by COA ANFIS.

4. Conclusions

It has been discovered that the artificial rabbit optimization (ARO), cuckoo optimization algorithm (COA) and grey wolf optimization (GWO) have a positive effect on the coupling between ANFIS system; so that innovative design patterns may be developed, two hybrid ANFIS models optimized with ARO, COA, and GWO have been used in the present article to use experimental data to estimate the driven piles' bearing capacity. To improve the modeling efficacy of the best networks, optimization methods were deployed to determine the essential parameters of the simulations, which were then applied. Also, other algorithms were developed for comparison purposes, such as single $ANFIS$, support vector regression (SVR) M5P, multiadaptive regression spline (MARS), random forests (RF), and random tree (RT). In order to measure a network's load capacity (Q_t), variables like hammer drop height (H), hammer weight (W), pile diameter (D), pile length (L), permanent penetration of a pile formed by the last hammer blow (S), and modulus of elasticity (E_p) has been utilized as input data. It was determined to split the material into two groups at random, one for analysis and the other for training, with 75% and 25% of the data distribution going to each group. The following are the primary findings:

- In addition to quantitative productivity indicators like $R^2, RMSE, MAE, RAE$, and RRSE, it is evident that both ANFIS systems optimized with ARO, GWO and COA accomplish admirably among the categories of trains and tests, with a minimum R^2 of 0.9285 in the learning dataset and 0.9313 in the examining dataset, respectively, indicating a strong similarity between experimental and estimated Q_t.

- Comparing the results of the single and hybrid models, it is obvious that the highest performance belonged to ARO - ANFIS, by gaining the largest values of correlation metrics and the lowest values of error-based metrics. The values of $R^2$for outp erformed model

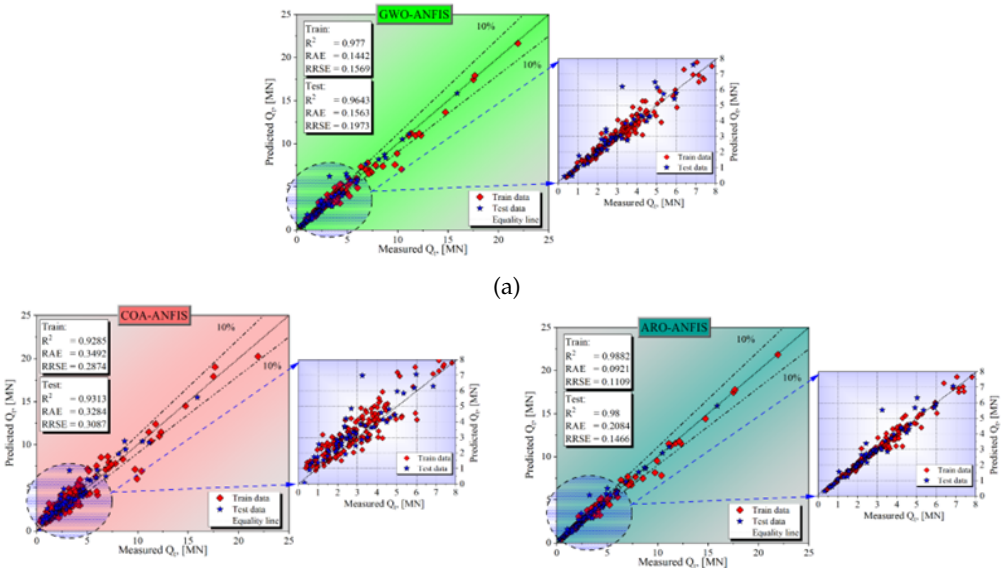

Fig. 4. The outputs of systems: a) GWO - ANFIS, b) COA - ANFIS, c) ARO - ANFIS

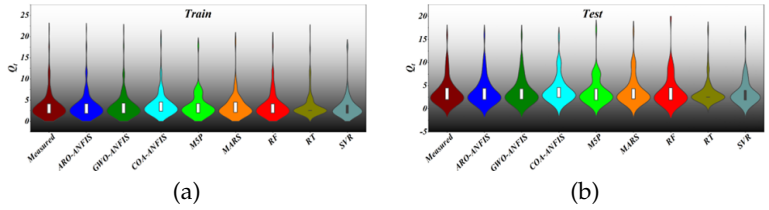

Fig. 5. The violin plots of the Q_t values from observations compared to those of developed models.

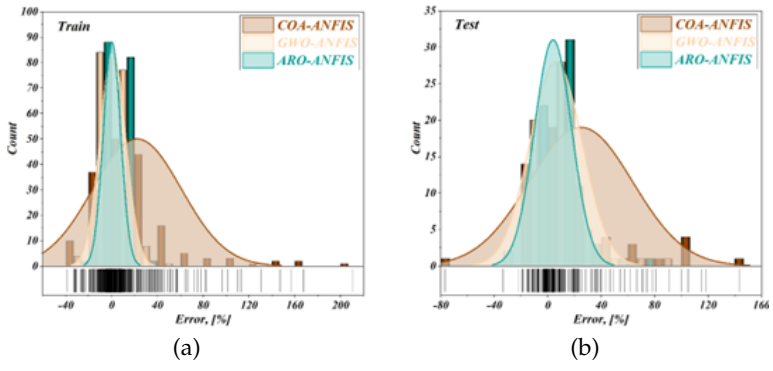

Fig. 6. The performance of systems considering error percentage, a) Train, b) Test

Table 4. The workability of generated systems

Category	Metric	Frameworks								
		ANFIS	COA-ANFIS	GWO - ANFIS	ARO - ANFIS	M5P	MARS	***RF***	***RT***	SVR
Train	R^2	0.9011	0.9285	0.977	0.9882	0.8109	0.8333	0.9037	0.8017	0.9174
	Rank score		1	2	3					
	RMSE	1.1304	0.9249	0.505	0.357	0.8575	0.8146	0.4434	0.9585	0.8573
	Rank score		1	2	3					
	MAE	0.8956	0.7117	0.2939	0.1876	0.8575	0.8146	0.4434	0.9585	0.5257
	Rank score		1	2	3					
	RAE	0.5025	0.3492	0.1442	0.0921	0.4208	0.3997	0.2176	0.4704	0.2583
	Rank score		1	2	3					
	RRSE	0.3961	0.2874	0.1569	0.1109	0.438	0.4104	0.3107	0.4453	0.2974
	Rank score		1	2	3					
	SI	0.2855	0.2511	0.1371	0.0969	0.3828	0.3586	0.2715	0.3891	0.2395
	Rank score		1	2	3					
Test	R^2	0.9089	0.9313	0.9643	0.98	0.8696	0.9125	0.9088	0.8163	0.7687
	Rank score		1	2	3					
	RMSE	1.092	0.89	0.5686	0.4226	1.0512	0.9305	1.0532	1.2372	1.632
	Rank score		1	2	3					
	MAE	0.853	0.6684	0.3181	0.2084	0.738	0.711	0.4995	0.9317	0.753
	Rank score		1	2	3					
	RAE	0.4902	0.3284	0.1563	0.1024	0.3625	0.3493	0.2454	0.4577	0.3695
	Rank score		1	2	3					
	RRSE	0.3199	0.3087	0.1973	0.1466	0.2937	0.26	0.2943	0.3457	0.5071
	Rank score		1	2	3					
	SI	0.2811	0.2487	0.1589	0.1181	0.2937	0.26	0.2943	0.0.3457	0.4431
	Rank score		1	2	3					
Total ranking score			12	24	36					

equal to 0.9882 and 0.98 related to ARO - $ANFIS$ for the training and testing stages, respectively.

- Considering other error-based metrics, the same behavior is validated with superiority of ARO - ANFIS, by receiving smaller values of RMSE, MAE, RAE, RRSE, and SI respect to other models. Regarding the second-best model, it is clear that the GWO - ANFIS system's results are near to the best model with slight differences, followed by COA - ANFIS . Although the COA - ANFIS 's performance was weaker than the other two hybrid ANFIS models, its accuracy was higher than single $ANFIS$ and the single analysis.
- It was obvious from error percentage distribution plots that the ARO - ANFIS system concluded the best performance by narrower distribution and restricted upper and lower bounds. After this, the performance of GWO - ANFIS is roughly similar to ARO - ANFIS but slightly weaker. Finally, the workability of the COA ANFIS depicted the wider normal distribution and smaller peak point around zero percentage.
- The developed models' comparison provided in the Taylor diagram for the training and testing stages showed that the ARO - ANFIS could obtain the closer point to reference point in both train and test stages, then GWO - ANFIS, followed by COA - ANFIS.
- After examining the dependability and considering the assumptions, it is clear that the ANFIS paired with ARO outperform the COA-ANFIS and GWOANFIS, which is the system that the Q_t of driven piles forecasting model recommends.

5. Acknowledgement

This work was supported by The Key University Science Research Project of Anhui Province (Grant No. 2023AH052675 and 2023AH052678).

References

[1] S. Adhikari and S. Bhattacharya, (2008) *"Dynamic Instability of Pile-Supported Structures in Liquefiable Soils during Earthquakes"* **Shock and Vibration *15***: 665–685. DOI: https://doi.org/10.1155/2008/149031.

[2] Q. Yang, S. Cheng, and B. Zhou, (2020) *"Monitoring study on vertical bearing capacity of pile foundation in soft rock of lhasa human settlements"* **Journal of Intelligent & Fuzzy Systems *38***: 7639–7650. DOI: https://doi.org/10.3233/JIFS-179834.

[3] S. A. Hoor and M. Esmaeili-Falak, (2024) *"Innovative Approaches for Mitigating Soil Liquefaction: A State-of-the-Art Review of Techniques and Bibliometric Analysis"* **Indian Geotechnical Journal**: 1–28. DOI: https://doi.org/10.1007/s40098-024-01120-3.

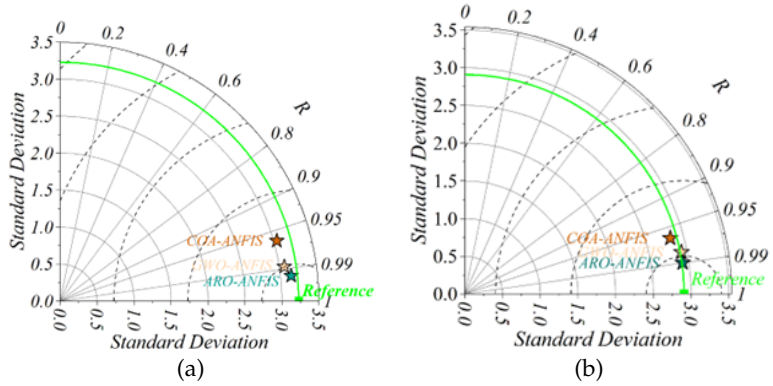

Fig. 7. The performance of systems considering Taylor diagram analysis

[4] P. O. V. Impe, W. F. V. Impe, and L. Seminck, (2013) *"Discussion of an instrumented screw pile load test and connected pile group load settlement behavior"* **Journal of Geo-Engineering Sciences *1***: 13–36. DOI: https://doi.org/10.3233/JGS-130011.

[5] B. B. Sheil, B. A. McCabe, C. E. Hunt, and J. M. Pestana, (2015) *"A practical approach for the consideration of single pile and pile group installation effects in clay: numerical modelling"* **Journal of Geo-Engineering Sciences 2**: 119–142. DOI: https://doi.org/10.3233/JGS-140027.

[6] G. Moradi, E. Hassankhani, and A. M. Halabian, (2022) *"Experimental and numerical analyses of buried box culverts in trenches using geofoam"* **Proceedings of the Institution of Civil Engineers-Geotechnical Engineering *175***: 311–322. DOI: https://doi.org/10.1680/jgeen.19.00288.

[7] B. Fellenius. *Basics of foundation design*. Lulu. com, 2017.

[8] A. Taghavi, A. Patil, and M. Davidson, (2017) *"Design-oriented seismic soil-pile-superstructure interaction analysis using a dynamic py method"* **Bridge Structures *13***: 57–67. DOI: https://doi.org/10.3233/BRS-170113.

[9] M. Esmaeili-Falak and R. S. Benemaran, (2024) *"Application of optimization-based regression analysis for evaluation of frost durability of recycled aggregate concrete"* **Structural Concrete *25***: 716–737. DOI: https://doi.org/10.1002/suco.202300566.

[10] J. E. Bowles and Y. Guo. *Foundation analysis and design*. ***5***. McGraw-hill New York, 1996.

[11] H. A. de Azeredo, (1977) *"O edifício até sua cobertura"* **Edgard Blucher Ltda, São Paulo**:

[12] B. M. Das and K. Sobhan, (1990) *"Principles of geotechnical engineering"*: 1–156.

[13] B. M. Das and N. Sivakugan. *Principles of foundation engineering*. Cengage learning, 2018.

[14] A. B. Vesic, (1963) *"Bearing capacity of deep foundations in sand"* **Highway research record**:

[15] F. Saberi-Movahed, M. Najafzadeh, and A. Mehrpooya, (2020) *"Receiving more accurate predictions for longitudinal dispersion coefficients in water pipelines: training group method of data handling using extreme learning machine conceptions"* **Water Resources Management *34***: 529–561. DOI: https://doi.org/10.1007/s11269-019-02463-w.

[16] G. Zhao, H. Wang, and Z. Li, (2023) *"Capillary water absorption values estimation of building stones by ensembled and hybrid SVR models"* **Journal of Intelligent & Fuzzy Systems *44***: 1043–1055. DOI: https://doi.org/10.3233/JIFS-221207.

[17] G. Yang, T. Li, C. Ma, L. Meng, H. Zhang, and J. Ma, (2022) *"Intelligent rating method of tunnel surrounding rock based on one-dimensional convolutional neural network"* **Journal of Intelligent & Fuzzy Systems *42***: 2451–2469. DOI: https://doi.org/10.3233/JIFS-211718.

[18] K. Zhang, Y. Zhang, and B. Razzaghzadeh, (2024) *"Application of the optimal fuzzy-based system on bearing capacity of concrete pile"* **Steel and Composite Structures *51***: 25–41. DOI: https://doi.org/10.12989/scs.2024.51.1.025.

[19] Y. Dawei, Z. Bing, G. Bingbing, G. Xibo, and B. Razzaghzadeh, (2023) *"Predicting the CPT-based pile set-up parameters using HHO-RF and PSO-RF hybrid models"* **Structural Engineering and Mechanics, An Int'l Journal *86***: 673–686. DOI: 10.12989/sem.2023.86.5.673.

[20] R. Liang and B. Bayrami, (2023) *"Estimation of frost durability of recycled aggregate concrete by hybridized Random Forests algorithms"* **Steel and Composite Structures *49***: 91–107. DOI: https://doi.org/10.12989/scs.2023.49.1.091.

[21] H. Kou, J. Quan, S. Guo, and E. Hassankhani, (2024) *"Light and normal weight concretes shear strength estimation using tree-based tunned frameworks"* **Construction and Building Materials *452***: 138955. DOI: https://doi.org/10.1016/j.conbuildmat.2024.138955.

[22] X. Sun, X. Dong, W. Teng, L. Wang, and E. Hassankhani, (2024) *"Creation of regression analysis for estimation of carbon fiber reinforced polymer-steel bond strength"* **Steel and Composite Structures *51***: 509–527. DOI: https://doi.org/10.12989/scs.2024.51.5.509.

[23] M. A. Shahin, M. B. Jaksa, and H. R. Maier, (2001) *"Artificial neural network applications in geotechnical engineering"* **Australian geomechanics *36***: 49–62.

[24] F. P. Nejad and M. B. Jaksa, (2017) *"Load-settlement behavior modeling of single piles using artificial neural networks and CPT data"* **Computers and Geotechnics *89***: 9–21. DOI: https://doi.org/10.1016/j.compgeo.2017.04.003.

[25] R. Jiang, (2022) *"Using the integrated neural network of radial basis function (RBF) via optimization algorithms to estimate pile settlement range"* **Journal of Intelligent & Fuzzy Systems *43***: 6683–6695. DOI: https://doi.org/10.3233/JIFS-220741.

[26] M. Zhang, Q. Du, J. Yang, and S. Liu, (2022) *"Modeling the pile settlement using the Integrated Radial Basis Function (RBF) neural network by Novel Optimization algorithms: HRBF-AOA and HRBF-BBO"* **Journal of Intelligent & Fuzzy Systems *43***: 7009–7022. DOI: https://doi.org/10.3233/JIFS-221021.

[27] T. Xia, W. Wang, and X. N. Wang, (2010) *"Artificial neural network model for time-dependent vertical bearing capacity of preformed concrete pile"* **Applied mechanics and materials *29***: 226–230. DOI: https://doi.org/10.4028/www.scientific.net/AMM.29-32.226.

[28] B. T. Kim, Y. S. Kim, and S. H. Lee, (2001) *"Prediction of lateral behavior of single and group piles using artificial neural networks"* **KSCE Journal of Civil Engineering *5***: 185–198. DOI: https://doi.org/10.1007/BF02829074.

[29] I. Alkroosh and H. Nikraz, (2014) *"Predicting pile dynamic capacity via application of an evolutionary algorithm"* **Soils and Foundations *54***: 233–242. DOI: https://doi.org/10.1016/j.sandf.2014.02.013.

[30] W. Zhang and A. T. C. Goh, (2016) *"Multivariate adaptive regression splines and neural network models for prediction of pile drivability"* **Geoscience Frontiers *7***: 45–52. DOI: https://doi.org/10.1016/j.gsf.2014.10.003.

[31] A. T. C. Goh, (1996) *"Pile driving records reanalyzed using neural networks"* **Journal of Geotechnical Engineering *122***: 492–495. DOI: https://doi.org/10.1061/(ASCE)0733-9410(1996)122:6(492).

[32] H. Ardalan, A. Eslami, and N. Nariman-Zadeh, (2009) *"Piles shaft capacity from CPT and CPTu data by polynomial neural networks and genetic algorithms"* **Computers and Geotechnics *36***: 616–625. DOI: https://doi.org/10.1016/j.compgeo.2008.09.003.

[33] I. S. Alkroosh, M. Bahadori, H. Nikraz, and A. Bahadori, (2015) *"Regressive approach for predicting bearing capacity of bored piles from cone penetration test data"* **Journal of Rock Mechanics and Geotechnical Engineering *7***: 584–592. DOI: https://doi.org/10.1016/j.jrmge.2015.06.011.

[34] F. Milad, T. Kamal, H. Nader, and O. E. Erman, (2015) *"New method for predicting the ultimate bearing capacity of driven piles by using Flap number"* **KSCE Journal of Civil Engineering *19***: 611–620. DOI: https://doi.org/10.1007/s12205-013-0315-z.

[35] S. Suman, S. K. Das, and R. Mohanty, (2016) *"Prediction of friction capacity of driven piles in clay using artificial intelligence techniques"* **International Journal of Geotechnical Engineering *10***: 469–475. DOI: https://doi.org/10.1080/19386362.2016.1169009.

[36] H. Maizir. "Evaluation of shaft bearing capacity of single driven pile using neural network". In: *Proceedings of the international multiconference of engineers and computer scientists*. ***1***. 2017, 15–17.

[37] H. Moayedi and S. Hayati, (2019) *"Artificial intelligence design charts for predicting friction capacity of driven pile in clay"* **Neural Computing and Applications *31***: 7429–7445. DOI: https://doi.org/10.1007/s00521-018-3555-5.

[38] A. S. Ibrahim, A. A. Musa, A. Y. Abdulfatah, and A. Idris, (2023) *"Developing soft-computing regression model for predicting soil bearing capacity using soil index properties"* **Modeling Earth Systems and Environment *9***: 1223–1232. DOI: https://doi.org/10.1007/s40808-022-01541-0.

[39] M. A. Mu'azu, (2023) *"Hybridized artificial neural network with metaheuristic algorithms for bearing capacity prediction"* **Ain Shams Engineering Journal *14***: 101980. DOI: https://doi.org/10.1016/j.asej.2022.101980.

[40] M. Panahi, A. Gayen, H. R. Pourghasemi, F. Rezaie, and S. Lee, (2020) *"Spatial prediction of landslide susceptibility using hybrid support vector regression (SVR) and the adaptive neuro-fuzzy inference system (ANFIS) with various metaheuristic algorithms"* **Science of the Total Environment *741***: 139937. DOI: https://doi.org/10.1016/j.scitotenv.2020.139937.

[41] M. Y. Anshori, D. Rahmalia, T. Herlambang, and D. F. Karya. "Optimizing Adaptive Neuro Fuzzy Inference System (ANFIS) parameters using Cuckoo Search (Case study of world crude oil price estimation)". In: *Journal of Physics: Conference Series*. ***1836***. IOP Publishing, 2021, 012041. DOI: 10.1088/1742-6596/1836/1/012041.

[42] J. Piri and M. R. R. Kahkha, (2017) *"Prediction of water level fluctuations of Chahnimeh reservoirs in Zabol using ANN, ANFIS and cuckoo optimization algorithm"* **Iranian Journal of Health, Safety and Environment *4***: 706–715.

[43] J. Piri, K. Mohammadi, S. Shamshirband, and S. Akib, (2016) *"Assessing the suitability of hybridizing the Cuckoo optimization algorithm with ANN and ANFIS techniques to predict daily evaporation"* **Environmental Earth Sciences *75***: 1–13. DOI: https://doi.org/10.1007/s12665-015-5058-3.

[44] H. A. R. d. Castro Filho, (2013) *"Construction companies' perception of sustainability rating programs for housing construction projects: a case study of the Caixa Casa Azul Seal"*:

[45] M. S. Jayaweera, (2011) *"Capacity estimation of piles using dynamic methods"*: DOI: http://dl.lib.mrt.ac.lk/handle/123/1868.

[46] B. de Oliveira Lobo, (2005) *"Método de previsão de capacidade de carga de estacas: aplicação dos conceitos de energia do ensaio SPT"*:

[47] , (2020) *"Standard Test Methods for Deep Foundations Under Static Axial Compressive Load"* **ASTM International *04.08***: 1–15. DOI: 10.1520/D1143_D1143M-07R13E01.

[48] A. International, (2017) *"Standard Test Method for High-Strain Dynamic Testing of Deep Foundations"* ***04.08***: 1–10. DOI: 10.1520/D4945-17.

[49] R. S. Benemaran, (2023) *"Application of extreme gradient boosting method for evaluating the properties of episodic failure of borehole breakout"* **Geoenergy Science and Engineering *226***: 211837. DOI: https://doi.org/10.1016/j.geoen.2023.211837.

[50] M. A. Hir, M. Zaheri, and N. Rahimzadeh, (2023) *"Prediction of rural travel demand by spatial regression and artificial neural network methods (Tabriz County)"* **Journal of transportation research (Tehran) *20***: 367–386. DOI: 10.22034/tri.2022.312204.2970.

[51] B. M. Yaychi and M. Esmaeili-Falak, (2024) *"Estimating axial bearing capacity of driven piles using tuned random forest frameworks"* **Geotechnical and Geological Engineering *42***: 7813–7834. DOI: https://doi.org/10.1007/s10706-024-02952-9.

[52] D. E. Farrar and R. R. Glauber, (1967) *"Multicollinearity in regression analysis: the problem revisited"* **The Review of Economic and Statistics**: 92–107. DOI: https://doi.org/10.2307/1937887.

[53] R. Rajabioun, (2011) *"Cuckoo optimization algorithm"* **Applied soft computing *11***: 5508–5518. DOI: https://doi.org/10.1016/j.asoc.2011.05.008.

[54] S. Mirjalili, S. M. Mirjalili, and A. Lewis, (2014) *"Grey wolf optimizer"* **Advances in engineering software *69***: 46–61. DOI: https://doi.org/10.1016/j.advengsoft.2013.12.007.

[55] L. Wang, Q. Cao, Z. Zhang, S. Mirjalili, and W. Zhao, (2022) *"Artificial rabbits optimization: A new bio-inspired meta-heuristic algorithm for solving engineering optimization problems"* **Engineering Applications of Artificial Intelligence *114***: 105082. DOI: https://doi.org/10.1016/j.engappai.2022.105082.

[56] J. S. Tang, (1993) *"ANFIS: Adaptive network based fuzzy inference systems"* **IEEE Trans. Syst. Cybern *23***: 515–520. DOI: 10.1109/21.256541.

[57] M. Esmaeili-Falak, H. Katebi, M. Vadiati, and J. Adamowski, (2019) *"Predicting triaxial compressive strength and Young's modulus of frozen sand using artificial intelligence methods"* **Journal of Cold Regions Engineering *33***: 04019007. DOI: https://doi.org/10.1061/(ASCE)CR.1943-5495.0000188.